Structural Stability of Silicon-Carbon Composites and Boron-Substituted Silicon as Candidate Anode Materials for Sodium-Ion Batteries: A Molecular Dynamics Study

Aditya Kejriwal[1]

Received June 15, 2026
Accepted October 8, 2026
Electronic access November 15, 2026

Sodium-ion batteries are being researched as a low-cost and sustainable alternative to lithium-ion batteries. However, as cell design is being developed, there are questions about efficient electrode and electrolyte materials. Currently, carbon-based compounds are the leading anode material, but silicon's high specific capacity makes it efficient and its abundance in the crust makes it economically and environmentally ideal. This study employed atomistic simulations to research the use of silicon as sodium-ion battery anode material. Using the Atomic Simulation Environment (ASE) a carbon coated silicon nanoparticle, layered silicon-graphene composites, and boron-substituted silicon were modeled. Molecular Dynamics was performed at 300 K with a 1fs timestep to simulate 50 sodium insertion and removal cycles, assessing structural stability and volumetric changes. It was found that the spherical silicon-carbon nanoparticle showed the greatest stability among the structures tested, with almost no degradation and deformation within the tested 50 insertion/removal cycles. Doping with boron also showed improved stability relative to the layered composite, but there were still large cycle-to-cycle fluctuations and degradation. These findings suggest that spherical nanoparticle composites exhibit favorable structural stability under simulated sodium insertion and removal, and there should be further investigation into their electrochemical performance and optimal carbon-to-silicon ratio and structure.

Keywords: Sodium-Ion Batteries, Silicon Anodes, Molecular Dynamics, Silicon-Carbon Composite, Boron-substituted Silicon, Structural Stability, Charge Cycle

Introduction

Lithium-ion batteries are at the forefront of energy storage technologies today. Their flexibility of use lends to their many different applications such as EVs, grid-connected storage, and electronic devices[1–3]. They have a high round-trip efficiency between 85% and 95% and a suitable balance of power density and energy density[1,4]. They also have long lifecycles and are lightweight and safe[5,6]. But as demand grows, sodium-ion batteries are a sustainable alternative. Sodium is more than 1000 times more abundant in the Earth's crust at $\sim$2.36% compared to lithium at $\sim$0.002%[7]. The material cost for sodium is also an order of magnitude (10-20$\times$) cheaper than lithium carbonate[8].

The main components of a sodium-ion battery are a cathode, anode, and electrolyte. As cell design is being developed, material choice is crucial for improving efficiency. The leading class of materials for sodium-ion battery anodes is carbon-based compounds[9,10]. Materials such as hard carbon are widely studied due to high capacity, cycling stability, and conductivity[11,12]. However, hard carbon has a lower specific capacity compared to other high-capacity materials such as silicon. Specific capacities measured for hard carbon anodes are $\sim$350 mAh/g while for silicon anodes are up to $\sim$950 mAh/g[11,13]. It is important to note that this value is idealized as practical capacities are typically much lower due to weak Na-Si alloying behavior[13].

But there are also problems with silicon-based materials in sodium-ion batteries. Sodium's larger ion size leads to poor insertion kinetics[14]. Silicon is also prone to large volume changes due to sodiation, which leads to mechanical instability and degradation[15,16]. These issues can make it difficult to characterize silicon performance through experiments alone. Atomistic simulations can help fill this gap. Despite these challenges, silicon is still an attractive candidate due to its high theoretical capacity and abundance. Carbon coating, nanostructuring, and boron doping have each shown to mitigate volume expansion and improve structural stability in silicon anodes[17,18].

This study used Molecular Dynamics simulations to assess the stability of boron-substituted silicon and silicon-carbon composites as anode material in sodium-ion batteries. It looked at silicon with varying concentrations of boron atoms

[1] *The Kinkaid School, USA*

© The National High School Journal of Science 2026

inserted, layered composites with different spacing between silicon and carbon layers, and a nanoparticle with a silicon shell and carbon coating. This work compares the performances of these silicon materials with each other as well as to other materials being used. These findings contribute to the broader effort of identifying and optimizing silicon-based anodes as well as informing future experimental and modeling work in sodium-ion battery development.

Methods

Crystalline silicon was modeled as a cubic structure with a diamond lattice. A lattice constant of 5.43 Å for silicon was used, consistent with reported values [19,20]. The crystalline structure consisted of 216 silicon atoms. Boron-substituted silicon was created by replacing silicon atoms with boron atoms. The addition of boron, which has one less valence electron, leads to electron holes, usually creating a p-type structure. However, this study used an MD calculator trained to reproduce atomic energies and forces. It does not explicitly model electronic structure, carrier density, Fermi level, or dopant charge state. These structures are therefore treated here as structural compositional analogs, and the term "p-type" is not used to describe simulation outcomes. This study used 3 concentrations: 1, 8, and 27 boron atoms, corresponding to around 0.463%, 3.705%, and 12.5% (Figure 1). The lowest concentration falls within the equilibrium solid solubility limit of boron in crystalline silicon [21]. The second concentration corresponds to boron concentration levels of ∼3-9% achieved experimentally via non-equilibrium techniques such as gas immersion laser doping and pulsed laser induced epitaxy which have been verified by atom probe tomography to form randomly distributed, non-clustered substitutional boron-silicon alloys well above the solubility limit [22]. The highest concentration exceeds boron levels demonstrated experimentally in literature and was chosen to more clearly resolve trends in the structural stability within the constraints of the 216-atom simulation cell. The layered composite was created by replacing crystalline silicon layers with graphene nano-ribbons. Structures with graphene replacing silicon every 3, 4, and 5 layers were tested (Figure 2) to sample a range of interlayer spacings spanning from tightly to loosely distributed graphene. This allowed the study to test the effect of graphene density on structure stability without the need for an exhaustive parameter sweep. Lastly, the nanoparticle composite was first created by carving the crystalline silicon into a sphere. Carbon atoms were then placed onto the silicon surface and relaxed to create a uniform coating (Figure 3).

Molecular Dynamics was then run to simulate repeated sodium insertion and removal using the Atomic Simulation Environment [24]. Sodium ions were repeatedly introduced and removed from the surface of the silicon structures and to simulate their interactions during cycling. In this context, one insertion/removal cycle was defined as the insertion of 10 sodium ions onto the silicon surface, equilibration for 1 ps, removal of the 10 sodium ions, and another 1 ps equilibration. Each cycle was a total of 2 ps with 1 fs timesteps. The sodium ions were initially randomly spaced onto one face of the boron-substituted silicon and layered composite structures (Figure 4). For the spherical composite, they were randomly spaced throughout the entire surface (Figure 5). In the simulation, the ions were free to migrate. Across the simulated

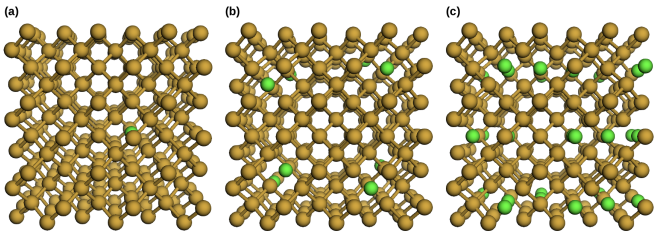


Figure. 1 Boron-substituted silicon created by substituting 1, 8, and 27 boron atoms into the silicon lattice, respectively. These correspond approximately to boron concentrations of 0.463%, 3.705%, and 12.5%. Images visualized using 3Dmol.js [23].

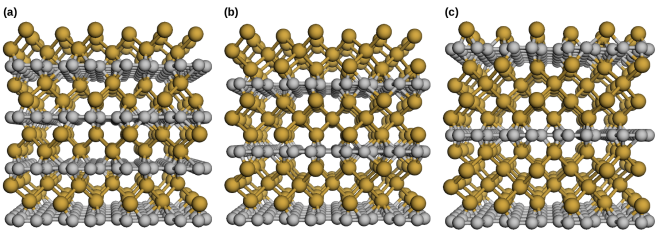


Figure. 2 Silicon-graphene layered composite with graphene nano-ribbons replacing silicon every 3, 4, and 5 layers, respectively.

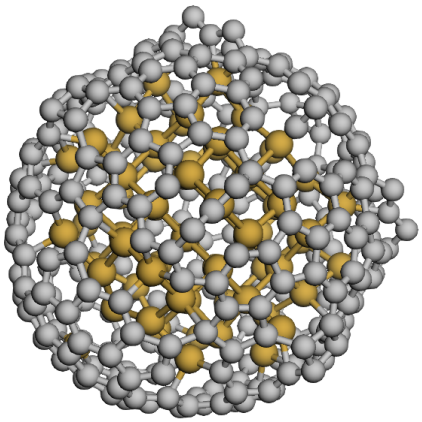


Figure. 3 Silicon-carbon nanoparticle with a crystalline silicon core and relaxed, uniform carbon shell.

© The National High School Journal of Science 2026

cycles, sodium ions partially diffused into the surface regions of the silicon structures rather than remain fixed. However, full penetration into the bulk of the structure was not observed within the simulated timescale. For each structure, 5 independent MD trials were run, with initial atomic velocities sampled from the Maxwell-Boltzmann distribution independently for each trial, and sodium ion placement randomized independently for each trial.

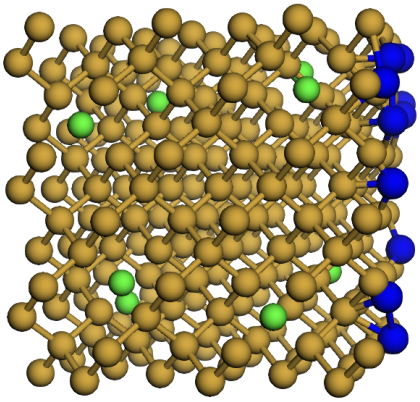


Figure. 4 Initial configuration of 10 sodium ions placed onto one face of a boron-substituted silicon structure prior to equilibration. This represents the starting point of a simulated cycle.

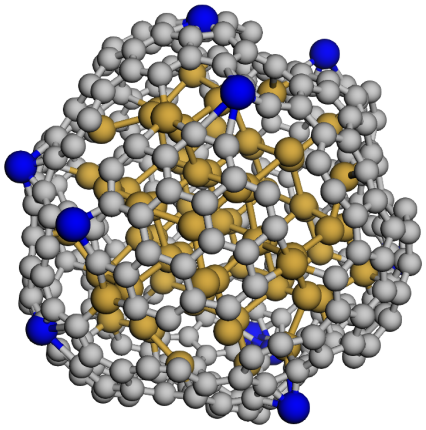


Figure. 5 Initial configuration of 10 sodium ions placed distributed across the surface of a silicon-carbon nanoparticle prior to equilibration.

After each cycle, the volume of each of the structures was estimated using an alpha-shape algorithm from the Open Visualization Tool (OVITO)[25]. This method tessellates space into tetrahedral simplices via Delaunay tessellation, approximating the outer boundary of a molecular structure by wrapping a surface around the atoms. This separates filled and void space to define the surface. The resulting mesh provides a representation of the structure's surface, which can then be used to calculate the volume (Figure 6).

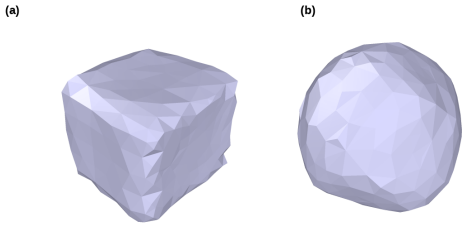


Figure. 6 Alpha-shape mesh used to estimate volume for the layered composite (first) and spherical composite (second), generated via Delaunay tessellation. Images visualized in OVITO.

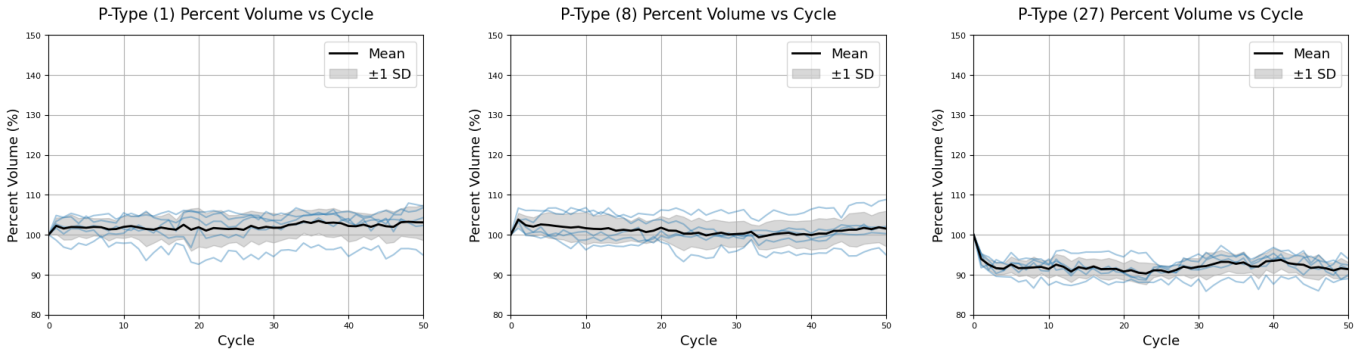
To run Molecular Dynamics, Velocity Verlet, an ASE library, was used. Velocity Verlet was chosen because of its stability during long simulations. In setting up the environment for the simulation, the Maxwell-Boltzmann distribution was needed as it describes initial velocities of particles based on a given temperature. MACE (Message Passing Atomic Cluster Expansion) was used as the Molecular Dynamics calculator[27]. MACE is a machine learning interatomic potential that predicts many-body atomic interactions using higher order equivariant message passing. It was selected for its near-DFT accuracy at a fraction of the computational cost, making it practical to run the repeated MD simulations (50 insertion/removal cycles across multiple structures). It captures the interactions relevant to Na-Si and Si-C that simpler force fields are not fitted to reproduce. Unlike conventional empirical force fields that rely on predefined functions and fitted parameters, MACE learns atomic interactions from quantum-mechanical reference data. This enables accurate predictions of energies and forces across a wide range of atomic configurations. This research used the MACE-MH-1 model with the OMAT PBE head[28]. Geometry relaxations used double-precision (float64) calculations to maximize accuracy. Molecular Dynamics used single-precision (float32) calculations. This improved computational efficiency while maintaining sufficient accuracy.

For more details regarding the example algorithms and visualization techniques employed, see the code in the data availability section.

Results

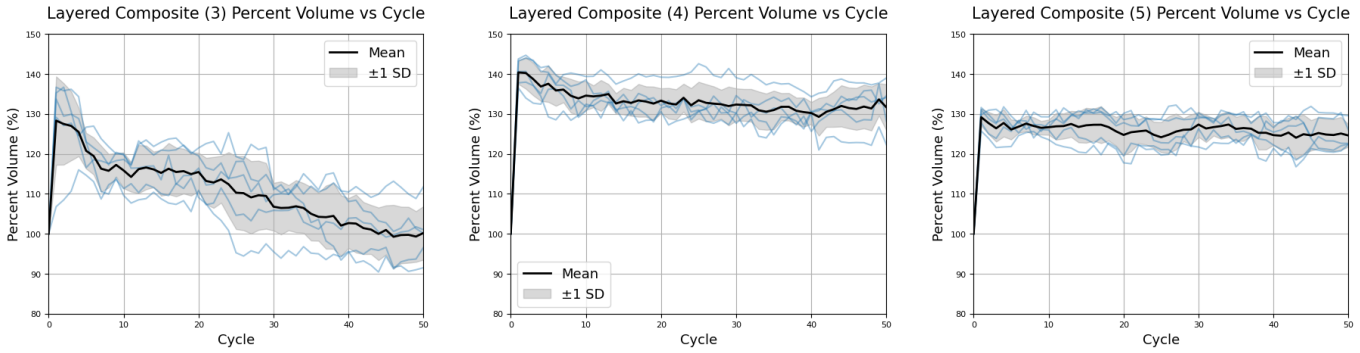
The analysis began by first finding the volume changes that occur during charge cycles. Sodium ions were repeatedly added and removed from the silicon surface a total of 50 times in order to simulate 50 different charge cycles. In between each cycle, an alpha-shape algorithm was used to calculate the volume of the structure. Sodium ions were observed to migrate into the surface region of each structure during equilibration,

© The National High School Journal of Science 2026



a b c

Figure. 7 Percent volume over 50 simulated cycles of boron-substituted silicon with 1, 8, and 27 boron atoms, respectively (n=5 independent trials per structure; shaded regions indicate ±1 standard deviation). The structures with 1 and 8 boron atoms show a final-cycle volume of 103.1% ± 4.5% and 101.5% ± 4.5%, respectively, with pronounced cycle-to-cycle fluctuations. The structure with 27 boron atoms shows an initial volume drop before stabilizing to a final-cycle volume of 91.4% ± 1.7%. Graphs made using Matplotlib[26].



a b c

Figure. 8 Percent volume over 50 simulated cycles of layered composite with graphene every 3, 4, and 5 layers, respectively (n=5 independent trials per structure; shaded regions indicate ±1 standard deviation). All structures show an initial spike in volume from graphene-silicon layer separation. Final-cycle volumes were 100.2% ± 6.7%, 131.6% ± 5.8%, and 124.6% ± 2.8%, respectively.

indicating partial subsurface intercalation. However, ions did not diffuse fully into the bulk of the structures within the simulated timescale, consistent with the short (2 ps) cycle duration discussed.

Boron-Substituted Silicon

For boron-substituted silicon, the structures with 1 and 8 boron atoms show a final-cycle volume of 103.1% ± 4.5% and 101.5% ± 4.5%, respectively (n=5), with pronounced cycle-to-cycle fluctuations of up to 5% of their original volume every cycle. The structure with 27 boron atoms behaved differently, showing an initial rapid volume drop before stabilizing to a final-cycle volume of 91.4% ± 1.7%, with similar cycle-to-cycle changes (Figure 7).

Silicon-Graphene Layered Composite

For the silicon-graphene layered composite, the volume initially spiked to 120-140%. This came from extreme expansion as the graphene and silicon layers separated. However, there were slight differences in behavior afterwards for each of the structures. The overall trend was that as graphene layers became more spaced, the amount the volume dropped after the spike decreased. Final-cycle volumes were 100.2% ± 6.7%, 131.6% ± 5.8%, and 124.6% ± 2.8% for graphene every 3, 4, and 5 layers, respectively (n=5). For the structure with graphene every 3 layers, the volume dropped closest to its original value; however, this did not mean it reformed into its original shape. Instead, the silicon between the graphene layers clumped, decreasing the volume while the layers still stayed separated. The structures with graphene every 4 and 5

© The National High School Journal of Science 2026

layers exhibited less clumping and remained further from their original volume.

Silicon-Carbon Nanoparticle

The most stable structure by far was the spherical Si-C composite. The final-cycle volume was 99.8% ± 0.6% (n=5), with no signs of mechanical degradation. Additionally, there were no signs of mechanical degradation. There was very slight deformation as the nanoparticle warped slightly into an ellipsoid from its original spherical shape, but the changes were minimal. In almost every trial, the cycle-to-cycle fluctuation was also less than 1%, demonstrating the stability of the composite (Figure 9).

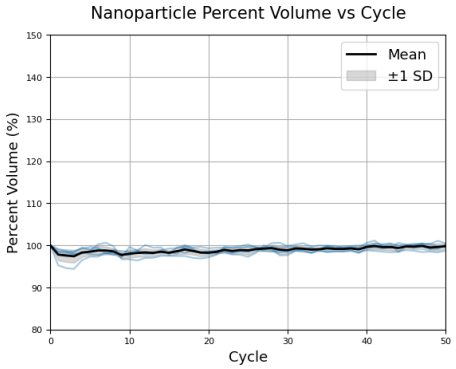


Figure. 9 Percent volume over 50 simulated cycles of a silicon-carbon nanoparticle (n=5 independent trials; shaded region indicates ±1 standard deviation). Final-cycle volume was 99.8% ± 0.6%, with no signs of mechanical degradation.

Discussion

The findings from this study's simulations offer insights about the use of silicon-carbon composites and boron-substituted silicon as anode material in sodium-ion batteries. To better understand these results, it is important to consider the structural factors underlying the observed trends. The results suggest a possible relationship between concentration and stability, though this trend was not isolated from other factors. Low concentrations lead to fluctuating volumes. Increasing dopant concentration did have a slight correlation with stability, but it also revealed that excessively high concentrations led to an initial period of instability. The layered Si-C composite revealed the instability of its interlayer interactions. Although Si-C is generally considered a stable compound, the layered structure was not able to maintain structural integrity, causing the layers to separate. However, the nanoparticle structure was well suited, undergoing minimal structural changes. The spherical shape distributed stress more evenly throughout the structure, nearly eliminating fluctuations in volume. This behaviour is consistent with established models that show spherical particles distribute strain radially and symmetrically, avoiding the stress concentrations that build at sharp edges and flat surfaces[29,30]. On the other hand, the layered composite's failure at its planar silicon-graphene interfaces matches known behavior in silicon electrodes as patterned or layered silicon electrode structures are prone to interfacial delamination under volumetric strain as stress concentrates at the boundary between different materials[31]. But, before drawing broader conclusions about silicon in real-world sodium-ion battery applications, some limitations in the simulation setup must be acknowledged.

A limitation present is that MACE-MH-1, the calculator used, does not explicitly model ionic charges. While electrostatic effects are implicitly taken into account as the model was trained on Density Functional Theory (DFT) calculations, the model does not treat sodium as an explicitly charged ion. Electrostatic interactions can influence ion stability, diffusion behavior, and insertion mechanisms, and the absence of an explicit treatment may affect the accuracy of the predicted sodium dynamics. Future studies could incorporate more accurate electrostatic potentials such as machine-learning models that explicitly take into account charge interactions or validate results against DFT calculations. This would provide a more realistic and accurate representation of the interactions between sodium ions and the silicon surface. In particular, benchmarking sodium adsorption energies, migration barriers, and Si-C/B-Si interfacial geometries against DFT, and confirming that the sub-1% volume stability reported for the nanoparticle is not an artifact of float32 numerical precision used during the MD production runs, would strengthen confidence in these results. Additionally, the 2 ps per simulated charge cycle is short, and may limit how much the sodium diffuses into the silicon structures or reaches equilibrium between insertion and removal steps. This timescale was chosen due to the computational cost of running 50 cycles across multiple structures. Longer simulation times per cycle would better capture realistic diffusion and relaxation behavior.

Another limitation of the simulations was that they did not fully factor in all elements of a realistic environment. The silicon and sodium ions were modeled without taking into account other key parts of a battery. For example, an electrolyte was not modeled, leaving out electrolyte nanoparticle and electrolyte-sodium ion interactions which would influence the behaviour in a real battery. Additionally, for the layered composite and boron-substituted silicon, the simulation assumed that the sodium ions were introduced on a single surface, enabling controlled assessment of structural changes but not fully capturing realistic sodiation behavior.

Several structural comparisons in this study were not fully isolated from other variables. The silicon-carbon nanoparti-

© The National High School Journal of Science 2026

cle combines both a carbon coating and a spherical geometry, and their individual contributions to stability were not tested separately, for example using an uncoated bare silicon sphere or a carbon-only reference structure. Similarly, the boron-substituted structures were not compared to an undoped crystalline silicon baseline under identical conditions, and a fixed Na loading of 10 ions was used across all structures regardless of differences in host-atom count and exposed surface area. As a result, the boron doping and nanoparticle geometry effects reported here should be interpreted as observed trends rather than isolated causal relationships. Disentangling these effects would require additional control structures (a bare silicon sphere, a carbon-only shell, an undoped silicon baseline). These additions were outside the scope and time constraints of this study and are recommended for future work.

Conclusions

This study examined the structural stability of silicon-carbon nanoparticles, silicon-graphene layered composites, and boron-substituted silicon under simulated sodium insertion and removal as a first step toward assessing their potential as sodium-ion battery anode candidates. The stability of the structure was tested over simulated sodium insertion/removal cycles. It was found that the spherical nanoparticle was the most stable, with a final-cycle volume of 99.8% ± 0.6% across 5 independent trials. Boron-substituted silicon followed, with the 1- and 8-boron structures ending near their original volume (103.1% ± 4.5% and 101.5% ± 4.5%, respectively) despite fluctuations of up to 10%, while the 27-boron structure stabilized to a lower final-cycle volume of 91.4% ± 1.7%. On the other hand, the layered composite was not suitable as its layers broke apart during sodiation.

Silicon-carbon spherical nanoparticles are already synthesizable via established routes such as wet chemical synthesis, chemical vapor deposition, and thermal plasma processing[32]. Prior mechanics-based modeling has shown that carbon shell thickness involves a trade-off between stability and specific capacity, suggesting that this study's nanoparticle structure should be further studied to optimize carbon-to-silicon ratio[33].

While the silicon-carbon nanoparticle was extremely stable, it is important to note that only 50 cycles were simulated. In real-life applications, batteries are expected to run hundreds to even thousands of cycles without significant volume changes. Longer simulations would have to be run in order to determine if this stability would persist over hundreds of cycles. Optimized silicon anodes in lithium-ion systems typically achieve structural retention of 80–85% after 100–200 cycles with surface modification strategies[34]. On the other hand, graphite anodes in lithium-ion batteries lose only 2-5% volume after 500-1000 cycles, and hard carbon anodes in sodium-ion batteries lose only 5-7% volume after 500 cycles[35,36].

The implications of this study are significant, especially as sodium-ion batteries emerge as an alternative to lithium-ion batteries. With sodium's natural abundance and favorable chemical properties, advances in this field could lead to more sustainable energy storage solutions. This research serves as a first look into the use of silicon-carbon composites and boron-substituted silicon anodes in enhancing sodium-ion battery performance. Further research should be done to optimize the performance of silicon-carbon nanoparticles, including simulations across a broader range of temperatures and sodium concentrations in order to better assess structural stability under practical conditions.

Data and Code Availability Statement

The code used to generate this data may be found at: `https://colab.research.google.com/drive/1x-3KiipNVGzihxj4AR_W0ucPRISvxDkX`

References

1 M. Martí-Florences, A. Cecilia, R. Costa-Castelló. Modelling and estimation in lithium-ion batteries: A literature review. Energies. Vol. 16, pg. 6846, 2023, https://doi.org/10.3390/en16196846.

2 B. Scrosati, J. Hassoun, Y. K. Sun. Lithium-ion batteries. A look into the future. Energy Environ. Sci. Vol. 4, pg. 3287–3295, 2011, https://doi.org/10.1039/C1EE01388B.

3 A. Masias, J. Marcicki, W. A. Paxton. Opportunities and challenges of lithium ion batteries in automotive applications. ACS Energy Lett. Vol. 6, pg. 621–630, 2021, https://doi.org/10.1021/acsenergylett.0c02584.

4 J. M. Tarascon, M. Armand. Issues and challenges facing rechargeable lithium batteries. Nature. Vol. 414, pg. 359–367, 2001, https://doi.org/10.1038/35104644.

5 G. E. Blomgren. The development and future of lithium ion batteries. J. Electrochem. Soc. Vol. 164, pg. A5019–A5025, 2017, https://doi.org/10.1149/2.0251701jes.

6 T. Horiba. Lithium-ion battery systems. Proc. IEEE. Vol. 102, pg. 939–950, 2014, https://doi.org/10.1109/JPROC.2014.2319832.

7 A. Sivakumaran, A. J. Samson, V. Thangadurai. Progress in sodium silicates for all-solid-state sodium batteries—A review. Energy Technol. Vol. 11, pg. 2201323, 2023, https://doi.org/10.1002/ente.202201323.

8 A. Yao, S. M. Benson. W. C. Chueh, Critically assessing sodium-ion technology roadmaps and scenarios for techno-economic competitiveness against lithium-ion batteries. Nature Energy. Vol. 10, pg. 404–416, 2025, https://doi.org/10.1038/s41560-024-01701-9.

9 J. F. Peters, M. Baumann, B. Zimmermann, J. Braun, M. Weil. The environmental impact of Li-ion batteries and the role of key parameters – A review. Renew. Sustain. Energy Rev. Vol. 67, pg. 491–506, 2017, https://doi.org/10.1016/j.rser.2016.08.039.

10 H. Hou. Carbon anode materials for advanced sodium-ion batteries. Adv. Energy Mater. Vol. 7, pg. 1602898, 2017, https://doi.org/10.1002/aenm.201602898.

11 C. Wu, Y. Yang, Y. Zhang, H. Xu, X. He, X. Wu, S. Chou. Hard carbon for sodium-ion batteries: progress, strategies and future perspective. Chem. Sci. Vol. 15, pg. 6244–6268, 2024, https://doi.org/10.1039/D4SC00734D.

© The National High School Journal of Science 2026

12 Y. Zheng, Y. Wang, Y. Lu, Y. Hu, J. Li. A high-performance sodium-ion battery enhanced by macadamia-shell-derived hard carbon anode. Nano Energy. Vol. 39, pg. 489-498, 2017, https://doi.org/10.1016/j.nanoen.2017.07.018.

13 F. K. Tareq, S. Rudra. Enhancing the performance of silicon-based anode materials for alkali metal (Li, Na, K) ion battery: A review on advanced strategies. Mater. Today Commun. Vol. 39, pg. 108653, 2024, https://doi.org/10.1016/j.mtcomm.2024.108653.

14 H. Zhang, I. Hasa, S. Passerini. Beyond insertion for na-ion batteries: nanostructured alloying and conversion anode materials. Adv. Energy Mater. Vol. 8, pg. 1702582, 2018, https://doi.org/10.1002/aenm.201702582.

15 L. C. Loaiza, L. Monconduit, V. Seznec. Si and ge-based anode materials for li-, na-, and k-ion batteries: a perspective from structure to electrochemical mechanism. Small. Vol. 16, pg. 1905260, 2020, https://doi.org/10.1002/smll.201905260.

16 C. Yang, S. Xin, L. Mai, Y. You. Materials design for high-safety sodium-ion battery. Adv. Energy Mater. Vol. 11, pg. 2000974, 2021, https://doi.org/10.1002/aenm.202000974.

17 G. F. Pach, P. R. Adhikari, J. Quinn, C. Wang, A. Singh, A. Verma, A. Colclasure, J. H. Kim, G. Teeter, G. M. Veith, N. R. Neale, G. M. Carroll. Boron–Silicon Alloy Nanoparticles as a Promising New Material in Lithium-Ion Battery Anodes. ACS Energy Lett. Vol. 9, pg. 2492–2499, 2024, https://doi.org/10.1021/acsenergylett.4c00856.

18 A. Bhowmick, X. Gao, W. Lu, J. Chakraborty, J. Xu. Multiscale electrochemo-mechanical model of high-capacity amorphous silicon anode material in sodium-ion batteries. Int. J. Solids Struct. Vol. 326, pg. 113753, 2026, https://doi.org/10.1016/j.ijsolstr.2025.113753.

19 T. Hom, W. Kiszenik, B. Post. Accurate lattice constants from multiple reflection measurements. II. Lattice constants of germanium, silicon, and diamond. J. Appl. Crystallogr. Vol. 8, pg. 459–464, 1975, https://doi.org/10.1107/S0021889875010965.

20 P. Becker, P. Scyfried, H. Siegert. The lattice parameter of highly pure silicon single crystals. Z. Phys. B Condens. Matter. Vol. 48, pg. 17–21, 1982, https://doi.org/10.1007/BF02026423.

21 G. L. Vick, K. M. Whittle. Solid Solubility and Diffusion Coefficients of Boron in Silicon. J. Electrochem. Soc. Vol. 116, pg. 1142–1144, 1969, https://doi.org/10.1149/1.2412239.

22 K. Hoummada, F. Dahlem, F. Panciera, E. Bustarret, C. Marcenat, D. Débarre, Y. El Amraoui, D. Mangelinck. Analysis of superconducting silicon epilayers by atom probe tomography: composition and evaporation field. Eur. Phys. J. Appl. Phys. Vol. 98, pg. 40, 2023, https://doi.org/10.1051/epjap/2023230018.

23 N. Rego, D. R. Koes. 3Dmol.js: molecular visualization with WebGL. Bioinformatics. Vol. 31, 1322–1324, 2015, https://doi.org/10.1093/bioinformatics/btu829.

24 A. H. Larsen, J. J. Mortensen, J. Blomqvist, I. E. Castelli, R. Christensen, M. Dułak, J. Friis, M. N. Groves, B. Hammer, C. Hargus, E. D. Hermes, P. C. Jennings, P. B. Jensen, J. Kermode, J. R. Kitchin, E. L. Kolsbjerg, J. Kubal, K. Kaasbjerg, S. Lysgaard, J. B. Maronsson, T. Maxson, T. Olsen, L. Pastewka, A. Peterson, C. Rostgaard, J. Schiøtz, O. Schütt, M. Strange, K. S. Thygesen, T. Vegge, L. Vilhelmsen, M. Walter, Z. Zeng, K. W. Jacobsen. The Atomic Simulation Environment—A Python library for working with atoms. J. Phys. Condens. Matter. Vol. 29, pg. 273002, 2017, https://doi.org/10.1088/1361-648X/aa680e.

25 A. Stukowski. Visualization and analysis of atomistic simulation data with OVITO–the Open Visualization Tool. Model. Simul. Mater. Sci. Eng. Vol. 18, pg. 015012, 2010, https://doi.org/10.1088/0965-0393/18/1/015012.

26 J. D. Hunter. Matplotlib: A 2D graphics environment. Comput. Sci. Eng. Vol. 9, pg. 90–95, 2007, https://doi.org/10.1109/MCSE.2007.55.

27 I. Batatia, D. P. Kovács, G. N. C. Simm, C. Ortner, G. Csányi. MACE: Higher Order Equivariant Message Passing Neural Networks for Fast and Accurate Force Fields. Advances in Neural Information Processing Systems. Vol. 35, pg. 11423–11436, 2022, https://doi.org/10.52202/068431-0830.

28 I. Batatia, C. Lin, J. Hart, E. Kasoar, A. M. Elena, S. W. Norwood, T. Wolf, G. Csányi. Cross Learning between Electronic Structure Theories for Unifying Molecular, Surface, and Inorganic Crystal Foundation Force Fields. arXiv preprint arXiv:2510.25380. 2025, https://doi.org/10.48550/arXiv.2510.25380.

29 Y. T. Cheng, M. W. Verbrugge. Evolution of stress within a spherical insertion electrode particle under potentiostatic and galvanostatic operation. J. Power Sources. Vol. 190, pg. 453–460, 2009, https://doi.org/10.1016/j.jpowsour.2009.01.021.

30 S. Golmon, K. Maute, S. H. Lee, M. L. Dunn. Stress generation in silicon particles during lithium insertion. Appl. Phys. Lett. Vol. 97, pg. 033111, 2010, https://doi.org/10.1063/1.3467838.

31 H. Haftbaradaran, X. Xiao, M. W. Verbrugge, H. Gao. Method to deduce the critical size for interfacial delamination of patterned electrode structures and application to lithiation of thin-film silicon islands. J. Power Sources. Vol. 206, pg. 357–366, 2012, https://doi.org/10.1016/j.jpowsour.2012.01.145.

32 X. Zhang, R. Hayashida, M. Tanaka, T. Watanabe. Synthesis of carbon-coated silicon nanoparticles by induction thermal plasma for lithium ion battery. Powder Technol. Vol. 371, pg. 26–36, 2020, https://doi.org/10.1016/j.powtec.2020.05.084.

33 W. Li, Q. Wang, K. Cao, J. Tang, H. Wang, L. Zhou, H. Yao. Mechanics-based optimization of yolk-shell carbon-coated silicon nanoparticle as electrode materials for high-capacity lithium ion battery. Comp. Comm. Vol. 1, pg. 1-5, 2016, https://doi.org/10.1016/j.coco.2016.07.002.

34 A. Rehman, S. Saleem, S. Ali, S. M. Abbas, M. Choi, W. Choi. Recent advances in alloying anode materials for sodium-ion batteries: material design and prospects. Energy Mater. Vol. 4, pg. 400068, 2024, https://doi.org/10.20517/energymater.2024.06.

35 J. P. Pender, G. Jha, D. H. Youn, J. M. Ziegler, I. Andoni, E. J. Choi, A. Heller, B. S. Dunn, P. S. Weiss, R. M. Penner, C. B. Mullins. Electrode degradation in lithium-ion batteries. ACS Nano. Vol. 14, pg. 1243–1295, 2020, https://doi.org/10.1021/acsnano.9b04365.

36 S. Tan, H. Yang, Z. Zhang, X. Xu, Y. Xu, J. Zhou, X. Zhou, Z. Pan, X. Rao, Y. Gu, Z. Wang, Y. Wu, X. Liu, Y. Zhang. The progress of hard carbon as an anode material in sodium-ion batteries. Molecules. Vol. 28, pg. 3134, 2023, https://doi.org/10.3390/molecules28073134.

© The National High School Journal of Science 2026